

# Radio Mini-Halo Emission from Cosmic Rays in Galaxy Clusters and Heating of the Cool Cores

Yutaka Fujita<sup>1\*</sup> and Yutaka Ohira<sup>2</sup>

<sup>1</sup>*Department of Earth and Space Science, Graduate School of Science, Osaka University, 1-1 Machikaneyama-cho, Toyonaka, Osaka 560-0043, Japan*

<sup>2</sup>*Department of Physics and Mathematics, Aoyama Gakuin University, Fuchinobe, Chuou-ku, Sagami-hara 252-5258, Japan*

Accepted 1988 December 15. Received 1988 December 14; in original form 1988 October 11

## ABSTRACT

It has been proposed that the cool cores of galaxy clusters are stably heated by cosmic rays (CRs). If this is the case, radio mini-halos, which are often found in the central regions of cool core clusters, may be attributed to the synchrotron emission from the CRs. Based on this idea, we investigate the radial profiles of the mini-halos. First, using numerical simulations, we confirm that it is appropriate to assume that radiative cooling of the intracluster medium (ICM) is balanced with the heating by CR streaming. In these simulations, we assume that the streaming velocity of the CRs is the sound velocity of the ICM, and indicate that the heating is even more stable than the case where the streaming velocity is the Alfvén velocity. Then, actually assuming the balance between cooling and heating, we estimate the radial profiles of CR pressure in six clusters only from X-ray observations. Since the CR protons interact with the ICM protons, we can predict the radial profiles of the resultant synchrotron radiation. We compare the predictions with the observed radial profiles of the mini-halos in the six clusters and find that they are consistent if the momentum spectra of the CRs are steep. These results may indicate that the cores are actually being heated by the CRs. We also predict broad-band spectra of the six clusters, and show that the non-thermal fluxes from the clusters are small in hard X-ray and gamma-ray bands.

**Key words:** cosmic rays — galaxies: clusters: general — cooling flows — radiation mechanisms: nonthermal — galaxies: clusters: individual: A1835, A2029, A2390, Perseus, RXJ1347.5-1145, Ophiuchus

## 1 INTRODUCTION

Radio halos are diffuse radio emission that permeates clusters of galaxies (Feretti & Giovannini 2008). They are believed to be synchrotron radiation from cosmic rays (CRs) in the intracluster medium (ICM). Although their surface brightness is low, they are often extended on scales of  $\sim$ Mpc. Since they are generally found in merging clusters, some phenomena associated with cluster mergers, such as shocks and turbulence in the ICM, may be responsible for the acceleration of the CR particles (e.g. Jaffe 1977; Roettiger, Stone, & Burns 1999; Takizawa & Naito 2000; Fujita & Sarazin 2001; Ohno, Takizawa, & Shibata 2002; Fujita, Takizawa, & Sarazin 2003; Brunetti et al. 2004; Brunetti & Lazarian 2011).

Among the radio-halos, so-called mini-halos are exceptional. While they are small in number, they are found in the cool cores of cool core clusters, which have not been dis-

turbed by cluster mergers for a long time (e.g. Govoni et al. 2009; Murgia et al. 2009). Their size ( $\sim 100$  kpc) is small compared with ordinary radio halos. The relation between the radio luminosity and the size is less clear for the mini-halos compared with the ordinary halos (Murgia et al. 2009), which has made it difficult to find the origin of the mini-halos. Gitti, Brunetti, & Setti (2002) proposed that the radio synchrotron emission comes from CR electrons reaccelerated by turbulence in the ICM. Pfrommer & Enßlin (2004) argue that the electrons illuminating the mini-halos are of secondary origin; they are created through the interaction between CR protons and ICM protons. Fujita et al. (2007) also proposed that the CR protons producing the secondary electrons are accelerated at shocks around the central active galactic nuclei (AGNs) in clusters.

For cool cores, there is another mystery with the ICM. The radiative cooling time of the ICM in the cores is generally less than the age of the clusters, while that in the surrounding region is larger than the age. If there are no heating sources, the ICM in the core should cool

\* E-mail: fujita@vega.ess.sci.osaka-u.ac.jp

and cannot sustain the pressure from the surrounding. In this case, a gas flow toward the cluster centre should develop (a cooling flow; see Fabian 1994). However, X-ray observations have shown that the massive cooling flows are not developing in cluster cores (e.g. Ikebe et al. 1997; Makishima et al. 2001; Peterson et al. 2001; Tamura et al. 2001; Kaastra et al. 2001; Matsushita et al. 2002). Thus, some unknown heating sources prevent cooling flows from developing in the cores.

In cool cores, active AGNs interacting with the ICM are often observed (e.g. Fabian et al. 2000; McNamara et al. 2000; Blanton et al. 2001; McNamara et al. 2001; Mazzotta et al. 2002; Fujita et al. 2002; Johnstone et al. 2002; Kempner, Sarazin, & Ricker 2002; Takizawa et al. 2003; Fujita et al. 2004). Through the AGN activities, CRs may be accelerated around the AGNs. The CRs may transfer the energy generated by the AGNs to the surrounding ICM (e.g. Tucker & Rosner 1983; Rephaeli 1987; Rephaeli & Silk 1995; Colafrancesco, Dar, & De Rújula 2004; Pfrommer et al. 2007; Jubelgas et al. 2008). One of the transfer mechanisms is CR streaming (Rephaeli 1979; Boehringer & Morfill 1988; Loewenstein, Zweibel, & Begelman 1991; Guo & Oh 2008), in which CRs interacting with Alfvén waves move outwards in the cluster. The ICM is heated by the  $PdV$  work of the CRs. We have shown that the CRs can actually heat the ICM (Fujita & Ohira 2011, hereafter Paper I). The heating is fairly stable because it is not localised around the AGN, and the density dependence of the heating term is globally similar to the radiative cooling term. Moreover, the CR distribution is not much affected by the temporal change of the ICM distribution.

If CR protons are heating cores, they should produce non-thermal emissions through their interaction with the thermal protons in the ICM. In that case, the radio mini-halos could be closely related to the heating of the cores. We calculated non-thermal spectra of cool cores that are heated by the CR protons (Fujita & Ohira 2012, hereafter Paper II). We compared the results with the radio observations of the mini-halo in the Perseus cluster. We found that the momentum spectrum of the CRs must be steep so as to be consistent with the observations of the mini-halo. We also showed that the detection of non-thermal emissions from the CRs would be difficult in the hard X-ray and gamma-ray bands, because of the steep spectrum. Thus, it is desirable to find a way of studying the CR heating in more detail only in the radio band.

In this paper, we show that CR heating can be studied closely by the radial profiles of mini-halos. If the CRs are stably heating a cool core, radiative cooling must be balanced with the heating at each radius. Assuming they balance, we can determine the radial profile of the CR pressure using only X-ray data for a cluster. Once we obtain the CR pressure profile, we can predict the radial profile of synchrotron radiation from the CRs and we can compare the predicted profile with the observed one. The idea of using the balance between the radiative cooling and the CR heating has been proposed by Colafrancesco & Marchegiani (2008). They considered Coulomb and hadronic interactions as the CR heating. However, since it has been indicated that CR streaming is a much more effective heating source

(Guo & Oh 2008, Paper I), we consider the CR streaming as the heating source in cores.

This paper is organised as follows. In Section 2, we describe our model on the estimation of CR pressure and the non-thermal emissions from the CRs. In Section 3, we check whether the CR heating is actually balanced with the radiative cooling using the results of numerical simulations. In that section, we also show that the CR heating is even more stable if the streaming velocity of the CRs is the sound velocity of the ICM, compared to the case where the streaming velocity is the Alfvén velocity. In Section 4, we predict radial profiles of mini-halos and compare them with the observations. Finally, Section 5 is devoted to discussion and conclusions. Throughout this paper we assume a  $\Lambda$ CDM cosmology with  $H_0 = 71 \text{ km s}^{-1} \text{ Mpc}^{-1}$ ,  $\Omega_m = 0.27$ , and  $\Omega_\Lambda = 0.73$ . We consider protons as CRs unless otherwise mentioned.

## 2 MODELS

### 2.1 CR Pressure

If the heating via CR streaming is balanced with radiative cooling in a cool core, it must be

$$H_{\text{st}} \approx n_e^2 \Lambda(T, Z), \quad (1)$$

where  $n_e$  is the electron density of the ICM. The heating rate of the CR streaming is given by

$$H_{\text{st}} = -v_{\text{st}} \frac{\partial P_c}{\partial r}, \quad (2)$$

where  $v_{\text{st}}$  is the streaming velocity of the CRs, and  $P_c$  is the CR pressure (Paper I). In our models,  $\partial P_c / \partial r < 0$ . We approximate the cooling function  $\Lambda$  by

$$\begin{aligned} \Lambda(T, Z) = & 2.41 \times 10^{-27} \left[ 0.8 + 0.1 \left( \frac{Z}{Z_\odot} \right) \right] \left( \frac{T}{\text{K}} \right)^{0.5} \\ & + 1.39 \times 10^{-16} \left[ 0.02 + 0.1 \left( \frac{Z}{Z_\odot} \right)^{0.8} \right] \\ & \times \left( \frac{T}{\text{K}} \right)^{-1.0} \text{ erg cm}^3, \end{aligned} \quad (3)$$

where  $T$  is the temperature and  $Z$  is the metal abundance of the ICM. This function approximates the one derived by Sutherland & Dopita (1993) for  $T \gtrsim 10^5 \text{ K}$  and  $Z \lesssim 1 Z_\odot$ .

From equation (1), we obtain CR pressure:

$$P_c(r) = \int_r^{r_{\text{max}}} \frac{n_e^2 \Lambda}{v_{\text{st}}} dr, \quad (4)$$

where  $r_{\text{max}}$  is the radius where  $P_c$  approaches zero. Since  $n_e^2$  rapidly decreases outside the core, the integration is insensitive to the value if we assume that it is much larger than the core radius. Thus, we assume that  $r_{\text{max}} = 1 \text{ Mpc}$ .

CRs move outwards as a whole in the cluster with waves that scatter the CRs. If the waves are Alfvén waves, the streaming velocity  $v_{\text{st}}$  may be the Alfvén velocity  $v_A$ . However, it has been indicated that the CR streaming velocity may be much larger than the Alfvén velocity in hot ICM, because in hot plasma the Alfvén waves may suffer strong resonant damping at small wave lengths by thermal protons. In this case, the sound velocity  $c_s$  may be appropriate as the streaming velocity (Holman, Ionson, & Scott 1979;

Enßlin et al. 2011). In this paper, we mainly consider the case of  $v_{st} = c_s$ .

In this study, we do not discuss the injection of CRs into the ICM in detail. They may be directly injected at shocks (Fujita et al. 2007), or they may be transported by buoyant bubbles (Guo & Oh 2008). In the latter case, the bubbles are created through AGN activities, which also accelerate CRs around the bubbles. The bubbles contain the CRs and carry them from the AGN out to large distances. As the bubbles adiabatically rise, the CRs may escape from the bubbles into the ICM or they may be injected into the ICM through the shredding of the bubbles by Rayleigh-Taylor and Kelvin-Helmholtz instabilities. While the adiabatic expansion reduces the energies of CRs, it does not change the slope of the momentum spectrum. Observations have shown that the bubbles with a size of  $\sim 10$  kpc are often found at the centre of cores, while large scale ( $\sim 100$  kpc) shocks appear to be rare (e.g. Birzan et al. 2004; McNamara & Nulsen 2012). This may suggest that CR injection via bubbles is more common.

## 2.2 Synchrotron Emission from CRs

Although we can obtain  $P_c(r)$  from equation (4) for given temperature and density distributions and the streaming velocity, we need to specify the momentum spectrum of the CRs to calculate the synchrotron spectrum of the CRs. For that purpose, we adopt the following spectrum:

$$N(p, r) = A_{cr}(r)p^{-x}e^{-p/p_{max}}, \quad (5)$$

where  $p$  is the CR momentum,  $x$  is the index, and  $p_{max}$  is the cutoff momentum.

The hadronic loss of CR protons could modify the slope of the spectrum (e.g. Brunetti et al. 2004; Enßlin et al. 2007; Guo & Oh 2008). In our case, the escape time of CRs from the core ( $\sim 10^8$ – $10^9$  yr) is smaller than the cooling time via hadronic loss. Thus, we ignore the modification of the spectrum by the loss.

We assume that  $x$  and  $p_{max}$  do not depend on  $r$  (Paper II). On the other hand, the normalisation of the spectrum,  $A_{cr}(r)$ , depends on  $r$  and it is determined from the following equation for given  $P_c(r)$ :

$$P_c(r) = \frac{c}{3} \int_{p_{min}}^{\infty} \frac{p^2 N(p, r)}{\sqrt{p^2 + m^2 c^2}} dp. \quad (6)$$

We determine the cutoff momentum  $p_{max}$  assuming that the high-energy CRs are accelerated at shocks formed through the activities of the central AGN (see Paper II). The cutoff momentum is determined by the age of the shock, and  $p_{max}c \sim 10^5$  TeV if the energy input through an explosive activity of the AGN is  $\sim 10^{60}$  erg. Although the actual acceleration mechanism is not clear (e.g. CRs may be accelerated nearby the black hole and form jets; Sikora et al. 2005), the following results are not sensitive to  $p_{max}$ . The minimum momentum,  $p_{min}$ , will be set in Section 3.1. On the other hand, as will be shown later, the synchrotron spectrum and luminosity are sensitive to the index  $x$ .

Once we fix the momentum spectrum of the CRs at each radius, we can calculate synchrotron and other non-thermal emissions from secondary electrons that are generated through the interaction between CR protons and ICM

protons, and through the decay of charged pions. We can also calculate  $\pi^0$ -decay gamma-rays. We use the radiation model of Fang & Zhang (2008) and the proton-proton collision model of Karlsson & Kamae (2008); the details are described in Fujita et al. (2009).

## 3 COMPARISON WITH NUMERICAL SIMULATIONS

### 3.1 Balance between Heating and Cooling

Before we study real clusters, we investigate whether the results of numerical simulations are well approximated by equation (1). We calculate  $P_c(r)$  based on the models in Papers I and II, although we make a few modifications as follows. We adopt the gravitational potential and the initial ICM profile of Model LCRs in Paper II. This model is originally constructed to reproduce the observations of the Perseus cluster. We do not include thermal conduction, and the CR diffusion can be ignored. The CR streaming velocity  $v_{st}$  is the sound velocity  $c_s$ . We reevaluate the parameters for Coulomb and hadronic losses of CR protons. This is because although we found that the index must be large ( $x \sim 3$ ) in Paper II, the model we used to obtain  $P_c(r)$  in Paper II did not include the effect. The parameters of the losses are calculated as follows (see also Guo & Oh 2008).

The energy loss of a proton with velocity of  $v = \beta c$  by Coulomb loss is given by Mannheim & Schlickeiser (1994):

$$\left(\frac{dE_p}{dt}\right)_c = -4.96 \times 10^{-19} \left(\frac{n_c}{\text{cm}^{-3}}\right) \frac{\beta^2}{\beta^3 + x_m^3} \text{ erg s}^{-1}, \quad (7)$$

where  $x_m = 0.0286 (T/2 \times 10^6 \text{ K})^{1/2}$ . For the momentum spectrum (5), the overall Coulomb loss rate is

$$\begin{aligned} \Gamma_c &= \int_{p_{min}}^{\infty} N \left(\frac{dE_p}{dt}\right)_c dp \\ &= -7.3 \times 10^{-16} \left(\frac{n_e}{\text{cm}^{-3}}\right) \\ &\quad \times \left(\frac{e_c}{\text{erg cm}^{-3}}\right) \text{ erg s}^{-1} \text{ cm}^{-3}, \end{aligned} \quad (8)$$

where  $e_c$  is the CR energy density. In this subsection, we assume that  $x = 3$  and  $T = 8$  keV, which are the typical values for the clusters we later investigate. The minimum momentum is set to be  $p_{min}c = 137$  MeV, which corresponds to the kinetic energy of 10 MeV and was adopted by Guo & Oh (2008). Around this momentum, the Coulomb loss of a proton is maximum ( $\beta \sim x_m$  in equation [7]).

The energy-loss rate of a CR proton due to pion production is approximately given by

$$\left(\frac{dE_p}{dt}\right)_h \approx -0.5 n_N \sigma_{pp} c T_p \theta(p - p_{thr}), \quad (9)$$

where  $n_N$  is the nucleon density,  $\sigma_{pp}$  is the  $pp$  cross-section,  $p_{thr}$  is the threshold momentum,  $T_p$  is the kinetic energy of the proton, and  $\theta$  is the step-function (Enßlin et al. 2007). For  $n_N$ ,  $\sigma_{pp}$ , and  $p_{thr}$ , we adopted the ones used in Enßlin et al. (2007). The overall hadronic loss rate is

$$\begin{aligned} \Gamma_h &= \int_{p_{thr}}^{\infty} N \left(\frac{dE_p}{dt}\right)_p dp \\ &= -1.5 \times 10^{-17} \left(\frac{n_e}{\text{cm}^{-3}}\right) \end{aligned}$$

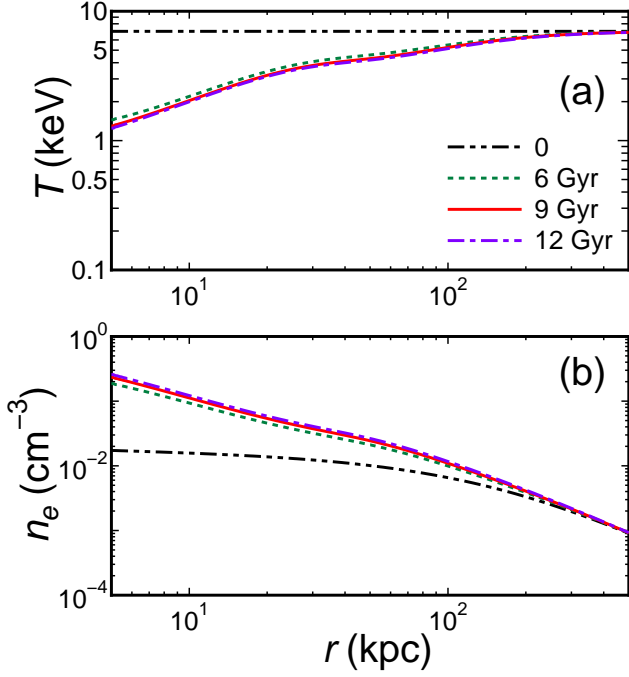


Figure 1. (a) Temperature and (b) density profiles for Model 1.

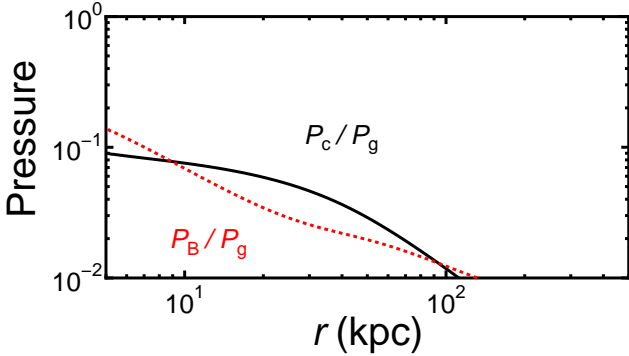


Figure 2. Profiles of the ratios  $P_c/P_g$  (solid) and  $P_B/P_g$  (dotted) at  $t = 9$  Gyr for Model 1.

$$\times \left( \frac{e_c}{\text{erg cm}^{-3}} \right) \text{ erg s}^{-1} \text{ cm}^{-3}. \quad (10)$$

Thus, the energy loss rate is  $\Gamma_{\text{loss}} = -\Gamma_c - \Gamma_h = \zeta_c n_c e_c$ , where  $\zeta_c = 7.5 \times 10^{-16} \text{ cm}^3 \text{ s}^{-1}$ . Since  $\sim 1/6$  of the inelastic energy goes into secondary electrons during hadronic collisions (Mannheim & Schlickeiser 1994; Guo & Oh 2008), the heating rate by the Coulomb and hadronic collisions is  $H_{\text{coll}} = -\Gamma_c - \Gamma_h/6 = \eta_c n_c e_c$ , where  $\eta_c = 7.4 \times 10^{-16} \text{ cm}^3 \text{ s}^{-1}$ . We use these values in equations (3) and (4) in Paper II. The values are not much different from the ones derived by Guo & Oh (2008) and adopted by us for  $x = 2.4$  using a slightly different formula ( $\zeta_c = 7.51 \times 10^{-16} \text{ cm}^3 \text{ s}^{-1}$  and  $\eta_c = 2.63 \times 10^{-16} \text{ cm}^3 \text{ s}^{-1}$ ).

In this subsection, we consider two models, which are based on Model LCRs in Paper II. Contrary to Model LCRs, we adopted the above  $\zeta_c$  and  $\eta_c$ . Moreover, we assume that the adiabatic index of the CRs is  $\gamma_c = 5/3$  instead of  $4/3$  as an extreme case, because the index approaches  $5/3$  if most

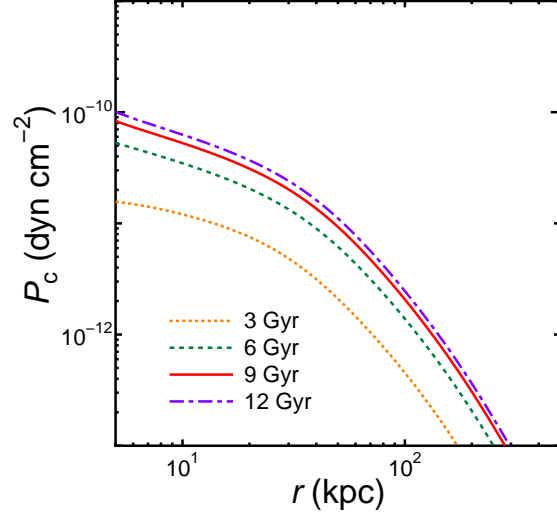


Figure 3. CR pressure profiles for Model 1.

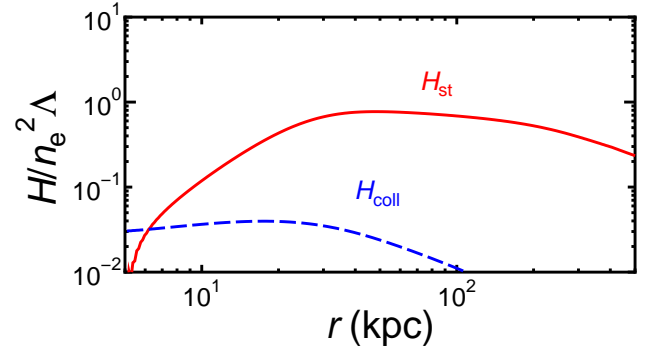


Figure 4. Relative importance of CR streaming ( $H_{\text{st}}$ ) and collisional heating ( $H_{\text{coll}}$ ) at  $t = 9$  Gyr for Model 1.

of the CRs have low energies. In Papers I and II, the total CR injection rate by the AGN was given by  $L_{\text{AGN}} = \epsilon \dot{M} c^2$ , where  $\dot{M}$  is the inflow rate of the gas toward the cluster centre. If the CRs are gradually injected into the ICM as the buoyant bubbles rise, their injection should not be localised. Thus, we give the CR injection rate per unit volume by  $\dot{S}_c \propto r^{-\nu}$  for  $20 \lesssim r \lesssim 150$  kpc. The lower bound is based on the observations of the bubbles (Birzan et al. 2004; Guo & Oh 2008). Although the upper bound is uncertain, the results are not sensitive to the value, because  $r^3 \dot{S}_c$  is a decreasing function of  $r$  if  $\nu > 3$ . In one model, we assume that the efficiency is  $\epsilon = 2.5 \times 10^{-4}$ , and the radial dependence is  $\nu = 3.1$ . These values are the same as those in Model LCRs in Paper II. We refer to this model as Model 1. We consider another model, which is the same as Model 1 but the AGN feedback is stronger (Model 2). We assume that  $\epsilon = 2.5 \times 10^{-3}$ , and that the energy input is more centrally concentrated ( $\nu = 3.5$ ). We have shown that the CR heating is locally unstable with these parameters ( $\epsilon$  and  $\nu$ ) if the streaming velocity is the Alfvén velocity and if thermal conduction is not included, because the heating is too strong and too centrally concentrated (Paper I). We assume that  $B = 10 (n_e/0.016 \text{ cm}^{-3})^{2/3} \mu\text{G}$ , which is the same as that in Model LCRs in Paper II.

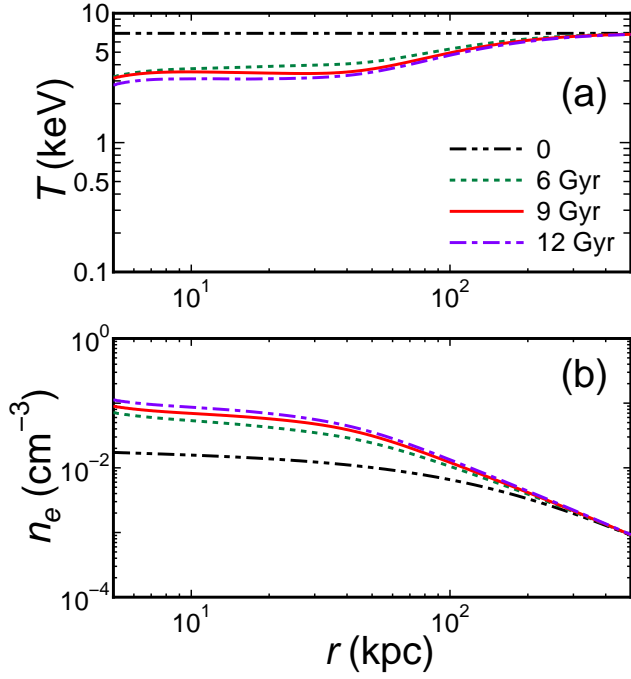


Figure 5. Same as Figure 1 but for Model 2.

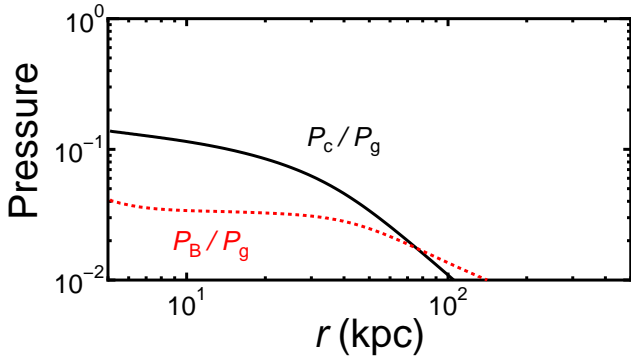


Figure 6. Same as Figure 2 but for Model 2.

It is to be noted that  $\dot{M}$  represents the mass flow that passes the inner boundary ( $r = 5$  kpc), and that not all the mass is swallowed by the central black hole. Most of the gas may be consumed by star formation in the central galaxy (e.g. McNamara & Nulsen 2012). For example, if 2.5% of  $\dot{M}$  goes to the neighbourhood of the black hole, and 10% of the rest mass energy is converted to CRs, the efficiency is  $\epsilon = 2.5 \times 10^{-3}$ . Although the conversion rate to CRs (10%) may be rather high, recent studies have shown that most of the AGNs at present seem to be in radiatively inefficient mode or radio mode (e.g. McNamara & Nulsen 2012), and that the inertia of AGN jets seems to be dominated by CR protons (Sikora et al. 2005). Thus, the conversion rate may not be unrealistic. The injected CRs eventually stream out of the cluster, to beyond the virial radius.

Figures 1–4 are the results for Model 1. Figures 1 and 2 are almost identical to the corresponding figures for Model LCRs in Paper II (Figures 8 and 9 in that paper). The cluster is isothermal and in hydro-statistic equilibrium

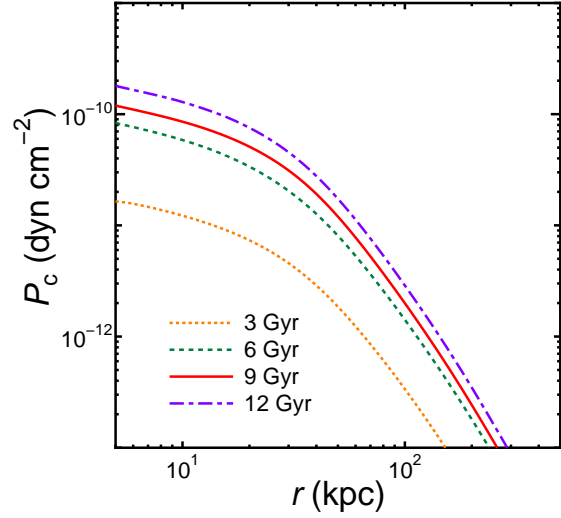


Figure 7. Same as Figure 3 but for Model 2.

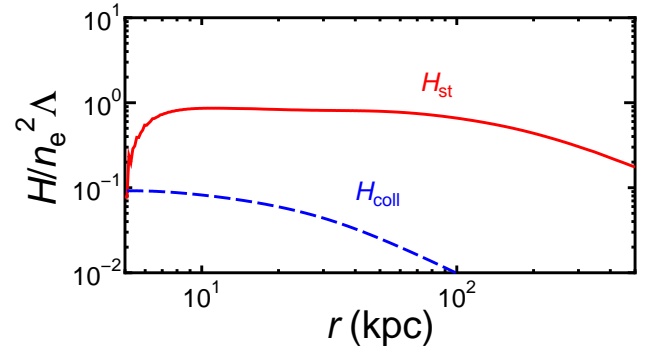


Figure 8. Same as Figure 4 but for Model 2.

at  $t = 0$  (Figure 1). The mass inflow rate gradually increases with time. At  $t = 12$  Gyr, the mass inflow rate is  $\dot{M} = 144 M_{\odot} \text{ yr}^{-1}$ . If there is no heating, it should be  $760 M_{\odot} \text{ yr}^{-1}$  (Paper I). In Figure 2, we show the ratios of the CR pressure  $P_c$  and the magnetic pressure  $P_B$  to the ICM pressure  $P_g$ . Figure 3 shows the evolution of

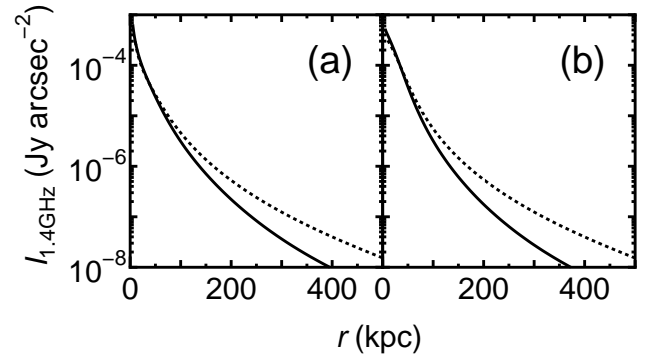


Figure 9. Profiles of synchrotron radiation when we use  $P_c(r)$  directly calculated via numerical simulations (solid lines) and when we use  $P_c(r)$  estimated by equation (4) (dotted lines). (a) Model 1 and (b) Model 2. The redshift of the cluster is set to be  $z = 0.0179$  (the Perseus cluster).

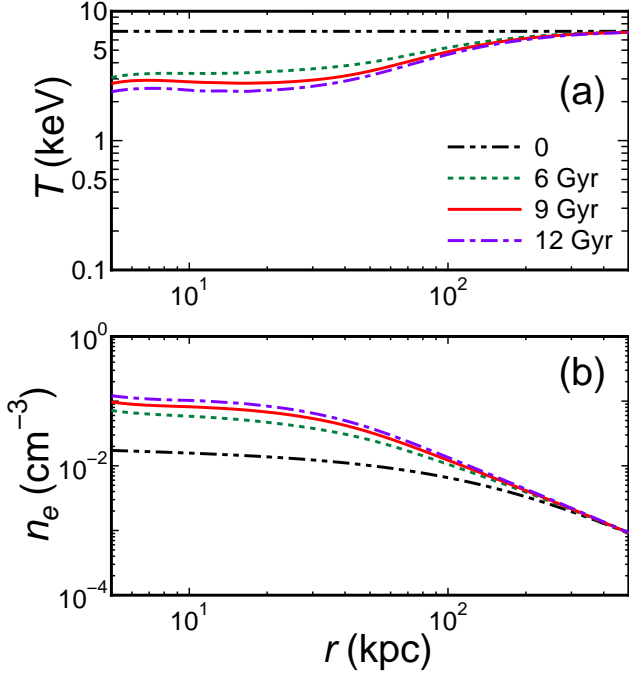


Figure 10. Same as Figure 1 but for Model 3.

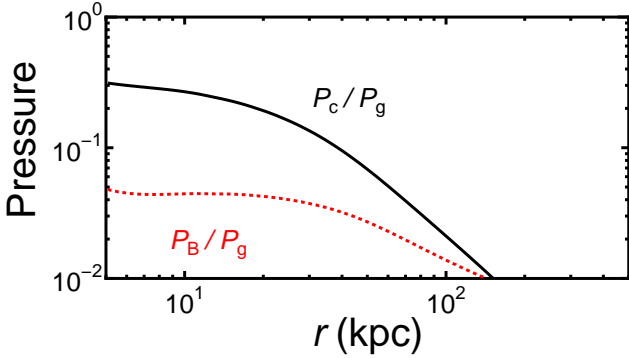


Figure 11. Same as Figure 2 but for Model 3.

$P_c(r)$ . For  $r \gtrsim 100$  kpc, the density of CRs nearly follows  $\rho_c \propto P_c^{1/\gamma_c} \propto r^{-2}$ , or  $P_c \propto r^{-10/3}$ . This is because of the continuity, almost constant sound velocity (streaming velocity), and inefficient cooling in the outer region of the cluster. However, the slope is less steep for  $r \lesssim 100$  kpc, because CRs are injected not at the cluster centre but mainly at  $20 \lesssim r \lesssim 150$  kpc. Figure 4 demonstrates that the CR heating,  $H_{st}$ , and radiative cooling,  $n_e^2 \Lambda$ , are well balanced except for the innermost and the outermost regions. The figure shows that  $0.5 \lesssim H_{st}/(n_e^2 \Lambda) < 0.8$  for  $20 \lesssim r \lesssim 200$  kpc. Figures 5–8 demonstrate the results for Model 2. The CR heating is stable in spite of the large  $\epsilon$  and  $\nu$ . This means that the CR heating with  $v_{st} = c_s$  is even more stable than that with  $v_{st} = v_A$ . Because of the strong feedback, radiative cooling is almost cancelled out. At  $t = 12$  Gyr, the mass inflow rate is only  $\dot{M} = 17 M_\odot \text{yr}^{-1}$ . The reason of the additional stability is that if the ICM temperature decreases at the cluster centre, the streaming velocity  $v_{st} = c_s$  decreases there. Thus, the escape of the CRs from the centre delays,

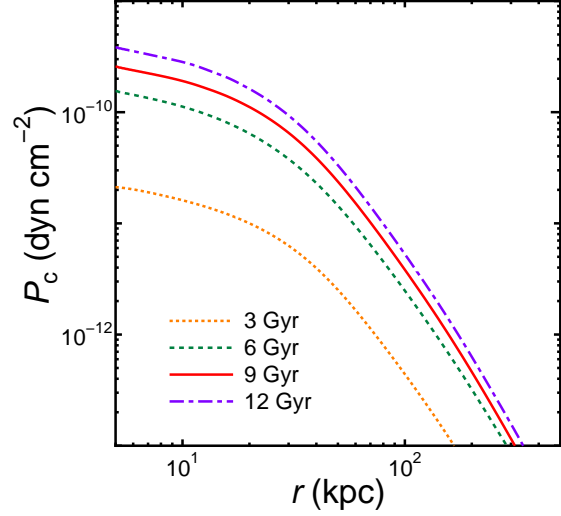


Figure 12. Same as Figure 3 but for Model 3.

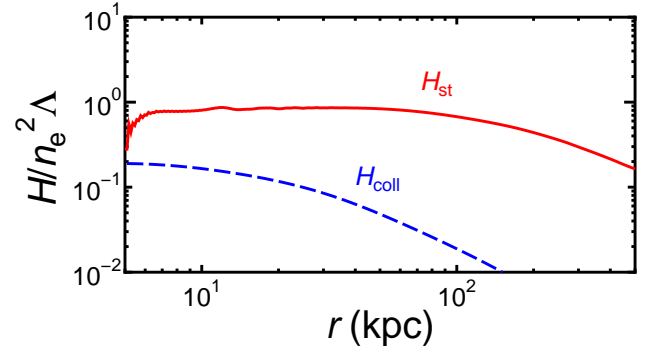


Figure 13. Same as Figure 4 but for Model 3.

which increases  $|dP_c/dr|$  and the heating rate (equation [2]). Figure 8 shows that  $0.7 \lesssim H_{st}/(n_e^2 \Lambda) < 1$  for  $r \lesssim 100$  kpc, and  $H_{st}/(n_e^2 \Lambda) \sim 0.5$  at  $r \sim 200$  kpc. The well-established balance between heating and cooling both for Models 1 and 2 suggests that the ICM evolves in such a way as to achieve the balance regardless of the details of the AGN heating model. In other words, equation (1) is the most important factor that determines the ICM profile in the core. It is to be noted that the bulk of CR energy is dissipated as heat within the core. In Model 2 for example, the CR energy injection rate from the AGN is  $2 \times 10^{45} \text{ erg s}^{-1}$  at  $t = 12$  Gyr. At the same time, the flux of CR enthalpy escaping the core (say, at  $r = 300$  kpc) is only  $4\pi\gamma_c v_{st} r^2 P_c/(\gamma_c - 1) \sim 3 \times 10^{44} \text{ erg s}^{-1}$ .

Figure 9 shows the radial profiles of synchrotron radio emission for Models 1 and 2 at  $t = 9$  Gyr. We chose  $x = 2.9$ , because the value is favourable when compared with observations (see Section 4.2). We compare the profiles that are calculated using  $P_c(r)$  in Figures 3 and 7 with those using  $P_c(r)$  derived from  $n_e(r)$ ,  $T(r)$ , and  $v_{st}(r) (= c_s(r))$  by equation (4). Figure 9 shows that their differences are small in the core region ( $r \lesssim 200$  kpc), which means that the approximation by equation (1) is good. However, outside the core region, the results using equation (4) is overestimated by a factor of a few, because the CR heating is not balanced with radiative cooling (Figures 4 and 8).

**Table 1.** Cluster profiles

Name	$z$	Profiles <sup>a</sup>	Refs
Perseus	0.0179	$n_e(r) = \frac{0.0193}{1+(r/18)^3} + \frac{0.046}{[1+(r/56)^2]^{1.8}} + \frac{0.0048}{[1+(r/197)^2]^{0.87}}$ $T(r) = 7.0 \frac{1+(r/70)^3}{2.3+(r/70)^3}$ $Z(r) = 0.46 + 0.27 \exp \left[ -\frac{1}{2} \left( \frac{r}{51} \right)^2 \right] - 0.42 \exp \left[ -\frac{1}{2} \left( \frac{r}{11} \right)^2 \right]$	$b$ $b$ $c$
A1835	0.2532	$n_e(r) = \frac{0.062}{[1+(r/41)]^{0.74}}$ (for $r \leq 231$ ) $n_e(r) = \frac{0.017}{[1+(r/158)]^{1.06}}$ (for $r > 231$ ) $T(r) = 7.8 - 3.7 \exp \left[ -\frac{1}{2} \left( \frac{r}{48} \right)^2 \right]$ $Z(r) = 0.28 + 0.15 \exp \left[ -\frac{1}{2} \left( \frac{r}{57} \right)^2 \right]$	$d$ $d$ $d$
A2029	0.0765	$n_e(r)^2 = (0.0168)^2 \frac{(r/85.5)^{-1.164}}{[1+(r/85.5)^2]^{1.05}} \frac{1}{[1+(r/923)^3]^{0.556}} + \frac{(0.376)^2}{[1+(r/5.08)^2]^3}$ $T(r) = 16.19 \frac{[(r/94.5)^{0.48} + 0.10]}{(r/94.5)^{0.48} + 1} \frac{(r/3088)^{0.03}}{[1+(r/3088)^{1.57}]^{3.76}}$ $Z(r) = 0.27 + 0.34 \exp \left[ -\frac{1}{2} \left( \frac{r}{96} \right)^2 \right]$	$e$ $e$ $f$
A2390	0.2280	$n_e(r) = 0.00385 \frac{(r/314)^{-0.9455}}{[1+(r/314)^2]^{0.5142}} \frac{1}{[1+(r/1223)^3]^{0.09383}}$ $T(r) = 19.34 \frac{[(r/218)^{0.08} + 0.12]}{(r/218)^{0.08} + 1} \frac{(r/2507)^{0.10}}{[1+(r/2507)^{5.0}]^{2.0}}$ $Z(r) = 0.33 + 0.42 \exp \left[ -\frac{1}{2} \left( \frac{r}{31} \right)^2 \right]$	$e$ $e$ $f$
RXJ1347	0.4510	$n_e(r) = \frac{0.25}{[1+(r/23.5)]^{0.78}}$ $T(r)$ is the curve shown in Figure 2 of reference $h$ $Z(r) = 0.33$	$g$ $h$ $i$
Ophiuchus	0.028	$n_e(r) = \frac{0.0127}{[1+(r/23.1)]^{1.11}} + \frac{0.0101}{[1+(r/162)]^{1.11}}$ $T(r) = 9.3 - 3.0 \exp \left[ -\frac{1}{2} \left( \frac{r}{19} \right)^2 \right]$ $Z(r) = 0.27 + 0.30 \exp \left[ -\frac{1}{2} \left( \frac{r}{27} \right)^2 \right]$	$j$ $j,k$ $j,k$

<sup>a</sup> The units for  $n_e$ ,  $T$ ,  $Z$ , and  $r$  are  $\text{cm}^{-3}$ , keV,  $Z_\odot$ , and kpc, respectively

<sup>b</sup> Mathews, Faltenbacher, & Brighenti (2006)

<sup>c</sup> Churazov et al. (2003)

<sup>d</sup> Majerowicz, Neumann, & Reiprich (2002)

<sup>e</sup> Vikhlinin et al. (2006)

<sup>f</sup> Vikhlinin et al. (2005)

<sup>g</sup> Allen, Schmidt, & Fabian (2002)

<sup>h</sup> Gitti, Piffaretti, & Schindler (2007)

<sup>i</sup> Ota et al. (2008)

<sup>j</sup> Nevalainen et al. (2009)

<sup>k</sup> Fujita et al. (2008)

### 3.2 Structure of the magnetic field

In our model, CRs are scattered by Alfvén waves. We have implicitly assumed that the gradient of  $P_c$  and the background magnetic field are parallel. However, magnetic field is often thought to be tangled in the ICM (Sarazin 1986), which may affect the CR streaming. It has been indicated that even if the gradient of  $P_c$  and the background magnetic field are not parallel, the plasma is unstable and waves are excited by CRs (Bell 2005; Rakowski, Laming, & Ghavamian 2008; Bykov, Osipov, & Ellison 2011; Rogachevskii et al. 2012). Thus, we expect that CRs are scattered by the waves. However, the effective streaming velocity for a tangled magnetic field is uncertain, and previous studies have not dealt with this problem (e.g. Loewenstein, Zweibel, & Begelman 1991; Guo & Oh 2008). Although the detailed study about it is

beyond the scope of our study, we investigate the effect in a simple way.

We assume that the streaming velocity for randomly tangled magnetic fields is reduced by a factor of  $\alpha$  from the one for the radially stretching magnetic field ( $v_{\text{st}} = \alpha c_s$ ). For a given magnetic field line, forward or backward Alfvén waves can exist. However, when the waves are excited by CRs, they are driven only in the direction closer to the CR pressure gradient, or outwards in a cluster in our case (e.g. Longair 1994). Owing to the scatter by the waves, a CR particle is not bound by a magnetic field line. On average, CRs move outwards along with the waves. If the angle between the magnetic field line and the direction of the CR pressure gradient is  $\theta$  ( $\leq \pi/2$ ), the effective wave velocity in the direction of the CR pressure gradient may be smaller than the sound velocity by a factor of  $\cos \theta$ , and  $\alpha$  may be

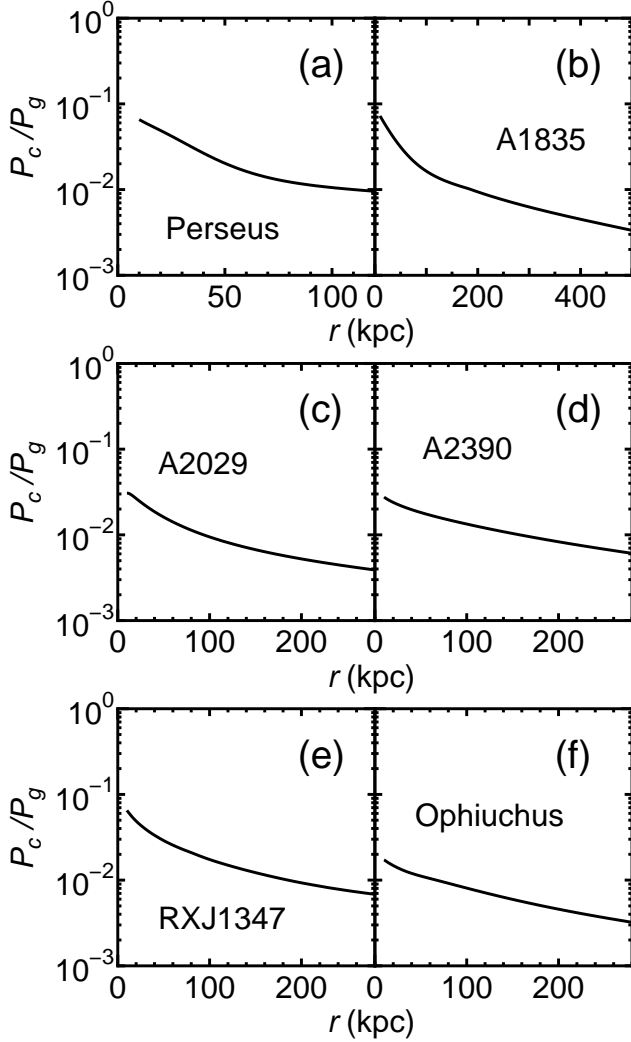


**Figure 14.** Ratio of CR pressure  $P_c$  to ICM pressure  $P_g$ .

the average of  $\cos \theta$ :

$$\alpha = \frac{\left( \int_0^{\pi/2} d\theta \sin \theta \int_0^{2\pi} d\phi \cos \theta \right)}{\left( \int_0^{\pi/2} d\theta \sin \theta \int_0^{2\pi} d\phi \right)} = 0.5. \quad (11)$$

Figures 10–13 show the results for the same parameters of Model 2 but for  $\alpha = 0.5$ . We refer to this model as Model 3. At  $t = 12$  Gyr, the mass inflow rate is  $\dot{M} = 16 M_\odot \text{ yr}^{-1}$ . The results are not much different from those of Model 2. However, the smaller streaming velocity makes the escape of CRs slower and increases  $P_c$  (Figures 7 and 12). It appears that the increase of  $P_c$  cancels out the decrease of  $v_{\text{st}}$  in equation (2). Since the difference between Models 2 and 3 is not significant, we assume that  $\alpha = 1$  in the following sections, unless otherwise mentioned.

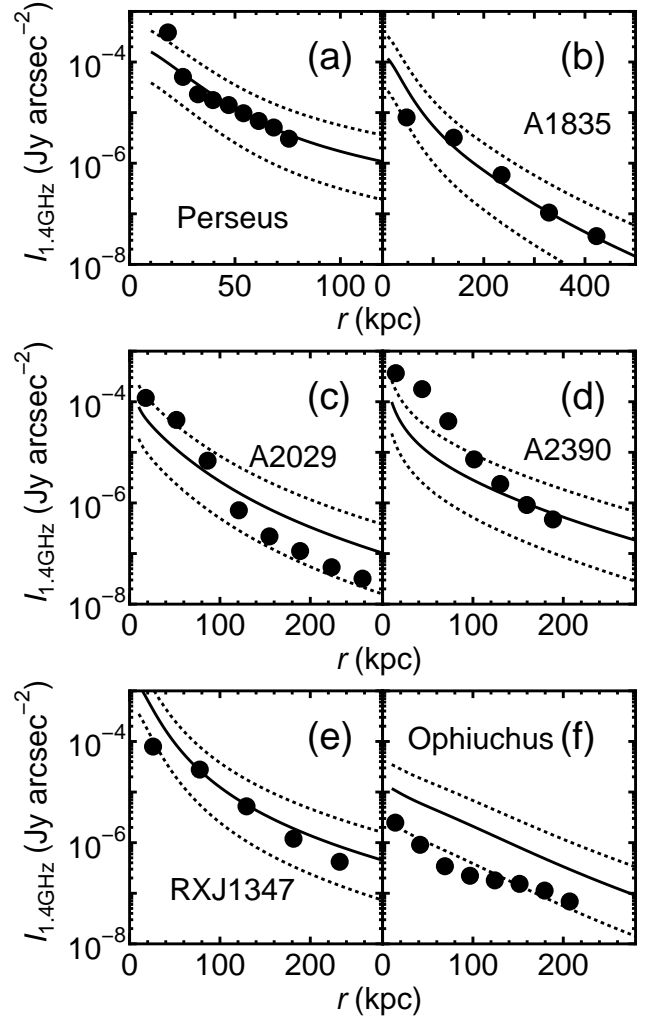


**Figure 15.** Predicted surface brightness profiles of synchrotron emission of the six clusters at  $\nu = 1.4$  GHz when  $v_{\text{st}} = c_s$  for  $x = 2.9$  (solid lines), 2.6 (upper dotted lines), and 3.3 (lower solid lines). Filled circles are the observations (Pedlar et al. 1990; Bacchi et al. 2003; Gitti et al. 2007; Murgia et al. 2009). Redshifts have been corrected.

## 4 COMPARISON WITH OBSERVATIONS

### 4.1 ICM models

We study six clusters (Perseus, A1835, A2029, A2390, RXJ1347, and Ophiuchus) for which the radial profiles of radio mini-halos have been studied in detail by Murgia et al. (2009, see also the references in the paper). We need to find  $n_e(r)$ ,  $T(r)$ , and  $Z(r)$  for the ICM of these clusters to obtain  $P_c(r)$  using equation (4). In Table 1, we show the ICM profiles we adopted. Some references give the functional forms. For other references, we fit the observational data with appropriate functions.

### 4.2 Results

Using the ICM models in Section 4.1, we can estimate  $P_c(r)$  by equation (4) for  $v_{\text{st}} = c_s$ . Figure 14 shows the ratio of CR pressure  $P_c$  to ICM pressure  $P_g$  for the six clusters. The ICM



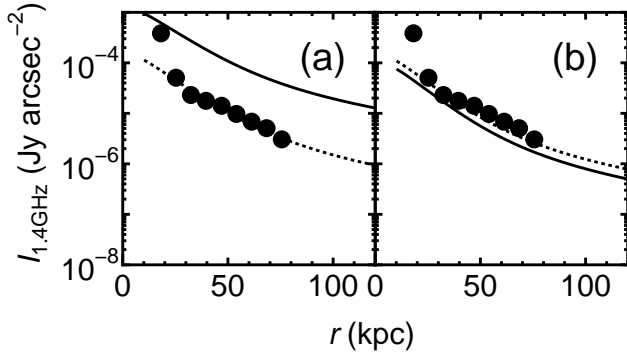


**Figure 16.** Profiles of synchrotron radiation of the Perseus cluster at  $\nu = 1.4$  GHz. (a) Streaming velocity is Alfvén velocity,  $v_A$ . The solid line shows  $x = 2.9$ , and the dotted line shows  $x = 3.5$ . (b)  $B = 3(n_e/0.016 \text{ cm}^{-3})^{2/3} \mu\text{G}$ . The solid line shows  $x = 2.9$ , and the dotted line shows  $x = 2.8$ . Filled circles are the observations (Pedlar et al. 1990; Murgia et al. 2009)

pressures are derived from the ICM models in Section 4.1. The CR pressures at the cluster centres are less than 10 %. In Figure 15, we show the predicted surface brightness profiles of synchrotron radiation for  $P_c$  shown in Figure 14. For these calculations, we need to specify  $B(r)$ . In Figure 15, we assume that  $B = 10(n_e/0.016 \text{ cm}^{-3})^{2/3} \mu\text{G}$ . For comparison, we show the observations (Murgia et al. 2009; Pedlar et al. 1990; Bacchi et al. 2003; Gitti et al. 2007). As can be seen, the observations are consistent with  $x \sim 2.9$ . The observations of all the six clusters are reproduced fairly well under the simple assumption of equation (1) and almost common index  $x \sim 3$ . In particular, the predicted slopes of the radial profiles are consistent with the observations, and the slopes are less uncertain than  $x$ . As was discussed in Section 3.1, the surface brightness may be overestimated a factor of few outside the core ( $r \gtrsim 200$  kpc). Even so, the agreement between the predictions and the observations is good. Among the six clusters, the consistency between the prediction and the observations of A2390 may be the worst (Figure 15d). Vikhlinin et al. (2006) indicated that the central region of the cluster is strongly disturbed by the central AGN, which might affect the results.

Figure 16 is the same as Figure 15a (Perseus) but for  $v_{st} = v_A$  (Figure 16a) and for a reduced magnetic field strength (Figure 16b). In general, the Alfvén velocity is smaller than the sound velocity in the ICM. Thus, when  $v_{st} = v_A$ , the escape of the CRs from the core delays and  $P_c$  becomes larger. Accordingly, for a given spectral shape, the synchrotron emission becomes larger than that in the case of  $v_{st} = c_s$  (the solid line in Figure 16a and that in Figure 15a). However, if we increase the spectral index to  $x = 3.5$ , the observations can be reproduced (the dotted line in Figure 16a). Although we do not present the result in the figure, we have also studied the profile for a reduced streaming velocity ( $v_{st} = 0.5c_s$ ). As is discussed in Section 3.2, the reduced velocity increases  $P_c$ . However, the effect is not significant, and the index of  $x = 3.0$  can reproduce the observations. In Figure 16b, we present the results when we reduced the magnetic field to  $B = 3(n_e/0.016 \text{ cm}^{-3})^{2/3} \mu\text{G}$ . The synchrotron emission reduces only a factor of a few for a spectral index of  $x \sim 3$  (the solid line in Figure 16b and that in Figure 15a). If we slightly reduce the index to  $x = 2.8$ ,

the observations are reproduced again (the dotted line in Figure 16b). Thus, the uncertainty of magnetic fields does not much affect the results.

In Figure 17, we present the broad-band spectra of the six clusters when  $v_{st} = c_s$ . We calculated non-thermal emissions from secondary electrons created through the decay of charged pions that are generated through the interaction between CR protons and ICM protons. We also calculated  $\pi^0$ -decay gamma-ray emissions. We did not include non-thermal emissions from primary electrons that are directly accelerated in the ICM, because we have no information on them. We adopted  $x = 2.9$  because it can fairly reproduce the radio profiles for the clusters (Figure 15). Figure 17 shows that except for the Perseus cluster, GeV gamma-ray fluxes are much smaller than  $10^{-12} \text{ erg cm}^{-2} \text{ s}^{-1}$ , which is the typical current upper limit set by *Fermi* (Ackermann et al. 2010). For the Perseus cluster, the contamination of the central AGN increases the upper-limit to  $\sim 10^{-11} \text{ erg cm}^{-2} \text{ s}^{-1}$  (Ackermann et al. 2010). Because of the steep CR momentum spectra, the fluxes in the hard X-ray band and the TeV gamma-ray band are small. Thus, the detection in these bands would be very difficult, which is consistent with recent TeV gamma-ray observations (e.g. Aleksić et al. 2012). If non-thermal emissions are observed in these bands in some clusters in the future, they might come from primary electrons.

## 5 DISCUSSION AND CONCLUSIONS

We have shown that the radial profiles of radio mini-halos observed in galaxy clusters can be explained by the synchrotron emission from the CRs that heat the cool cores of the clusters. In our model, the cores are being heated via CR streaming.

First, we investigated whether the CR heating is balanced with radiative cooling of the ICM using numerical simulations. We assumed that the streaming velocity of the CRs ( $v_{st}$ ) is the sound velocity of the ICM ( $c_s$ ), because it has been pointed out that it is more appropriate than Alfvén velocity ( $v_A$ ) in hot ICM. Moreover, we found that the heating is more stable when  $v_{st} = c_s$  than when  $v_{st} = v_A$ . We showed that the CR heating is actually balanced with the radiative cooling inside the core, although the heating falls short of the cooling a factor of a few outside the core.

Assuming that the CR heating is balanced with the cooling in the cores of six real clusters (Perseus, A1835, A2029, A2390, RXJ1347, and Ophiuchus), we estimated the radial profiles of CR pressure only from X-ray observations. The results showed that the CR pressure at the cluster centres are less than 10 %. Assuming that the momentum spectra of the CRs are given by a power-law and the CR streaming velocity is the sound velocity, we calculated radial profiles of the synchrotron emission from secondary electrons created through proton-proton interaction. We found that the profiles match the observations if the index of the CR momentum spectra is  $x \sim 3$ . If the CR streaming velocity is the Alfvén velocity, the index must be  $x \sim 3.5$  to be consistent with the observations. Uncertainties of magnetic fields in the ICM do not much affect the results. We have compared our predictions with the observations of only six clusters, and our model has free parameters such as  $x$ .

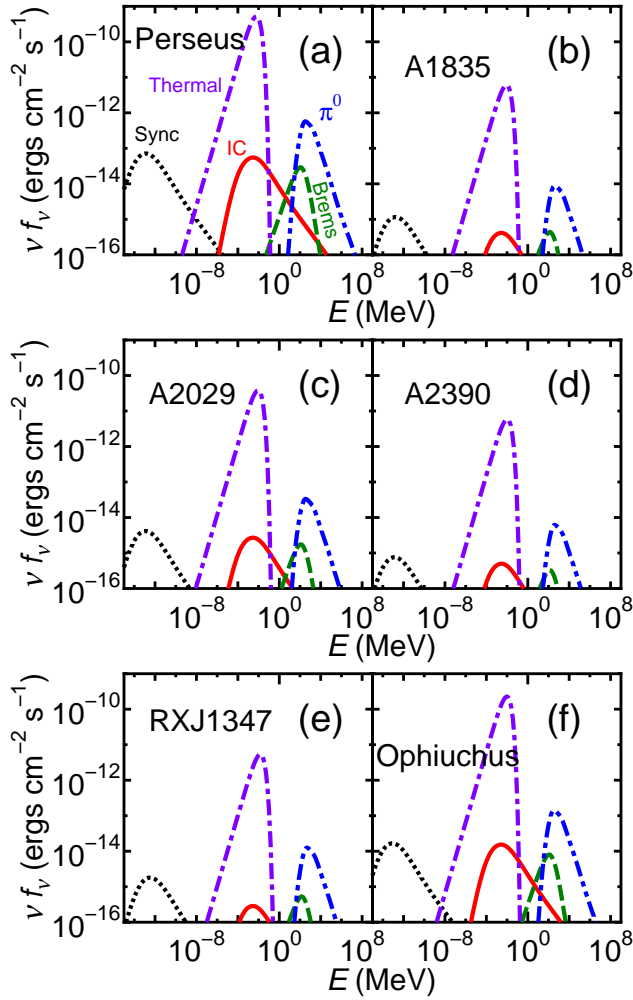


**Figure 17.** Broad-band spectra of the six clusters. Synchrotron radiation (dotted line), inverse Compton scattering off cosmic microwave background (solid line), and non-thermal bremsstrahlung (dashed line) are of the secondary electrons. The  $\pi^0$ -decay gamma-rays are shown by the two-dot-dashed line. For comparison, the thermal bremsstrahlung from the ICM is shown by the dot-dashed line. Redshifts have been corrected.

However, if radial profiles of mini-halos are studied for many other clusters in the future, our model can be examined more extensively through the comparison with the observations.

We also estimated broad-band spectra for the six clusters when  $x \sim 3$ . Owing to the steep spectra, hard X-ray and gamma-ray fluxes are small, which makes it difficult to detect the non-thermal emissions from the CRs in the clusters in those bands. In the radio band, future observations of the spectral index will give us information on the momentum spectra of CRs. For the Perseus cluster, we have shown that our predicted index is consistent with the observations (Paper II).

## ACKNOWLEDGMENTS

We thank the anonymous referee, whose comments greatly improved the clarity of this paper. We also thank F. Taka-

hara for useful discussion. This work was supported by KAKENHI (Y. F.: 23540308, Y. O.: 24.8344).

## REFERENCES

- Ackermann M., et al., 2010, *ApJ*, 717, L71  
 Aleksić J., et al., 2012, *A&A*, 541, A99  
 Allen S. W., Schmidt R. W., Fabian A. C., 2002, *MNRAS*, 335, 256  
 Bacchi M., Feretti L., Giovannini G., Govoni F., 2003, *A&A*, 400, 465  
 Bell A. R., 2005, *MNRAS*, 358, 181  
 Birzan L., Rafferty D. A., McNamara B. R., Wise M. W., Nulsen P. E. J., 2004, *ApJ*, 607, 800  
 Blanton E. L., Sarazin C. L., McNamara B. R., Wise M. W., 2001, *ApJ*, 558, L15  
 Boehringer H., Morfill G. E., 1988, *ApJ*, 330, 609  
 Brunetti G., Blasi P., Cassano R., Gabici S., 2004, *MNRAS*, 350, 1174  
 Brunetti G., Lazarian A., 2011, *MNRAS*, 412, 817  
 Bykov A. M., Osipov S. M., Ellison D. C., 2011, *MNRAS*, 410, 39  
 Churazov E., Forman W., Jones C., Böhringer H., 2003, *ApJ*, 590, 225  
 Colafrancesco S., Dar A., De Rújula A., 2004, *A&A*, 413, 441  
 Colafrancesco S., Marchegiani P., 2008, *A&A*, 484, 51  
 Enßlin T., Pfrommer C., Miniati F., Subramanian K., 2011, *A&A*, 527, A99  
 Enßlin T. A., Pfrommer C., Springel V., Jubelgas M., 2007, *A&A*, 473, 41  
 Fabian A. C., 1994, *ARA&A*, 32, 277  
 Fabian A. C., et al., 2000, *MNRAS*, 318, L65  
 Fang J., Zhang L., 2008, *MNRAS*, 384, 1119  
 Feretti L., & Giovannini, G. 2008, *A Pan-Chromatic View of Clusters of Galaxies and the Large-Scale Structure*, 740, 143  
 Fujita Y., et al., 2008, *PASJ*, 60, 1133  
 Fujita Y., Kohri K., Yamazaki R., Kino M., 2007, *ApJ*, 663, L61  
 Fujita Y., Ohira Y., 2011, *ApJ*, 738, 182 (Paper I)  
 Fujita Y., Ohira Y., 2012, *ApJ*, 746, 53 (Paper II)  
 Fujita Y., Ohira Y., Tanaka S. J., Takahara F., 2009, *ApJ*, 707, L179  
 Fujita Y., Sarazin C. L., 2001, *ApJ*, 563, 660  
 Fujita Y., Sarazin C. L., Kempner J. C., Rudnick L., Slee O. B., Roy A. L., Andernach H., Ehle M., 2002, *ApJ*, 575, 764  
 Fujita Y., Sarazin C. L., Reiprich T. H., Andernach H., Ehle M., Murgia M., Rudnick L., Slee O. B., 2004, *ApJ*, 616, 157  
 Fujita Y., Takizawa M., Sarazin C. L., 2003, *ApJ*, 584, 190  
 Gitti M., Brunetti G., Setti G., 2002, *A&A*, 386, 456  
 Gitti M., Ferrari C., Domainko W., Feretti L., Schindler S., 2007, *A&A*, 470, L25  
 Gitti M., Piffaretti R., Schindler S., 2007, *A&A*, 472, 383  
 Govoni F., Murgia M., Markevitch M., Feretti L., Giovannini G., Taylor G. B., Carretti E., 2009, *A&A*, 499, 371  
 Guo F., Oh S. P., 2008, *MNRAS*, 384, 251  
 Holman G. D., Ionson J. A., Scott J. S., 1979, *ApJ*, 228, 576

- Ikebe Y., et al., 1997, *ApJ*, 481, 660
- Jaffe W. J., 1977, *ApJ*, 212, 1
- Johnstone R. M., Allen S. W., Fabian A. C., Sanders J. S., 2002, *MNRAS*, 336, 299
- Jubelgas M., Springel V., Enßlin T., Pfrommer C., 2008, *A&A*, 481, 33
- Kaastra J. S., Ferrigno C., Tamura T., Paerels F. B. S., Peterson J. R., Mittaz J. P. D., 2001, *A&A*, 365, L99
- Karlsson N., Kamae T., 2008, *ApJ*, 674, 278
- Kempner J. C., Sarazin C. L., Ricker P. M., 2002, *ApJ*, 579, 236
- Loewenstein M., Zweibel E. G., Begelman M. C., 1991, *ApJ*, 377, 392
- Longair, M. S., 1994, *High Energy Astrophysics*, second edition, Cambridge Univ. Press, Cambridge, vol. 2, § 20.4
- Makishima K., et al., 2001, *PASJ*, 53, 401
- Majerowicz S., Neumann D. M., Reiprich T. H., 2002, *A&A*, 394, 77
- Mannheim K., Schlickeiser R., 1994, *A&A*, 286, 983
- Mathews W. G., Faltenbacher A., Brighenti F., 2006, *ApJ*, 638, 659
- Matsushita K., Belsole E., Finoguenov A., Böhringer H., 2002, *A&A*, 386, 77
- Mazzotta P., Kaastra J. S., Paerels F. B., Ferrigno C., Colafrancesco S., Mewe R., Forman W. R., 2002, *ApJ*, 567, L37
- McNamara B. R., et al., 2000, *ApJ*, 534, L135
- McNamara B. R., et al., 2001, *ApJ*, 562, L149
- McNamara B. R., Nulsen P. E. J., 2012, *NJPh*, 14, 055023
- Murgia M., Govoni F., Markevitch M., Feretti L., Giovannini G., Taylor G. B., Carretti E., 2009, *A&A*, 499, 679
- Nevalainen J., Eckert D., Kaastra J., Bonamente M., Kettula K., 2009, *A&A*, 508, 1161
- Ohno H., Takizawa M., Shibata S., 2002, *ApJ*, 577, 658
- Ota N., et al., 2008, *A&A*, 491, 363
- Pedlar A., Ghataure H. S., Davies R. D., Harrison B. A., Perley R., Crane P. C., Unger S. W., 1990, *MNRAS*, 246, 477
- Peterson J. R., et al., 2001, *A&A*, 365, L104
- Pfrommer C., Enßlin T. A., 2004, *A&A*, 413, 17
- Pfrommer C., Enßlin T. A., Springel V., Jubelgas M., Dolag K., 2007, *MNRAS*, 378, 385
- Rakowski C. E., Laming J. M., Ghavamian P., 2008, *ApJ*, 684, 348
- Rephaeli Y., 1979, *ApJ*, 227, 364
- Rephaeli Y., 1987, *MNRAS*, 225, 851
- Rephaeli Y., Silk J., 1995, *ApJ*, 442, 91
- Rogachevskii I., Kleeorin N., Brandenburg A., Eichler D., 2012, *ApJ*, 753, 6
- Roettiger K., Stone J. M., Burns J. O., 1999, *ApJ*, 518, 594
- Sarazin C. L., 1986, *RvMP*, 58, 1
- Sikora M., Begelman M. C., Madejski G. M., Lasota J.-P., 2005, *ApJ*, 625, 72
- Sutherland R. S., Dopita M. A., 1993, *ApJS*, 88, 253
- Takizawa M., Naito T., 2000, *ApJ*, 535, 586
- Takizawa M., Sarazin C. L., Blanton E. L., Taylor G. B., 2003, *ApJ*, 595, 142
- Tucker W. H., Rosner R., 1983, *ApJ*, 267, 547
- Tamura T., et al., 2001, *A&A*, 365, L87
- Vikhlinin A., Kravtsov A., Forman W., Jones C., Markevitch M., Murray S. S., Van Speybroeck L., 2006, *ApJ*, 640, 691
- Vikhlinin A., Markevitch M., Murray S. S., Jones C., Forman W., Van Speybroeck L., 2005, *ApJ*, 628, 655